Hindawi Publishing Corporation
Mathematical Problems in Engineering
Volume 2013, Article ID 935371, 7 pages
http://dx.doi.org/10.1155/2013/935371

Research Article

Real-Time Dry Beach Length Monitoring for Tailings Dams Based on Visual Measurement

Jun Hu,[1] Shan Hu,[1] Fei Kang,[2] and Jianhua Zhang[3]

[1] *School of Mining Engineering, University of Science and Technology Liaoning, Anshan, Liaoning 114051, China*
[2] *Faculty of Infrastructure Engineering, Dalian University of Technology, Dalian, Liaoning 116024, China*
[3] *College of Computer Science and Technology, Zhejiang University of Technology, Hangzhou, Zhejiang 310023, China*

Correspondence should be addressed to Jun Hu; kdhj1977@126.com

Received 18 August 2013; Accepted 4 October 2013

Academic Editor: Xiao-Wei Ye

The length of dry beach is an important factor that influences the safety of tailings dams. However, there still is no accurate and reliable method that can conveniently measure the length of dry beach. In this paper, the authors focus on developing a novel method for dry beach length determination. The proposed method can effectively measure the dry beach length through an ordinary camera and four marking rods placed on the dry beach. Experimental results show that the proposed method can conveniently measure the dry beach length with high accuracy, and therefore it can be adopted as an effective method in tailings dam real-time health monitoring.

1. Introduction

Increased awareness of the economic and social effects of aging, deterioration, and extreme events on civil infrastructure has been accompanied by recognition of the need for advanced structural health monitoring and damage detection tools [1]. Structural health monitoring is a technology that allows the estimation of the structural state and detection of structural change that affects the performance of a structure [2, 3]. Recently, many advanced measurement methods such as global positioning systems (GPS) [4, 5], wireless sensor networks [6, 7], and fiber Bragg grating sensing [8] have been adopted for health monitoring of engineering structures. Meanwhile, various signal processing methods such as particle filtering algorithm [9], wavelet thresholding [10], particle swarm optimization [11, 12], artificial bee colony algorithm [13], and neural networks [14] are developed to deal with the data obtained by the sensor systems to reflect the status of structures.

Tailings pond is formed by damming at valley interception or damming at all sides, which is used to store tailings and other industrial waste produced by metal and nonmetal mines. Tailings dams are a particular type of dam built to store mill and waste tailings from mining activities, and a tailings dam is an important part of a tailings pond, which refers to the initial dam and later fill dam. Tailings storage facilities are complex geotechnical structures. A number of singular characteristics make tailings dams more vulnerable than other types of retention structures. Many tailings dam failure cases have been reported [15]. The failure of a tailings dam may cause grave disasters such as floods [16] and groundwater pollution [17]. Therefore, in the design and operation stages of a tailings project, the stability of the tailings dam, the control capacity for flood, and the reliability of the drainage and safety monitoring facilities should be fully evaluated [18]. Some works of the literature have focused on the static and dynamic stability analysis of tailings structures [19–22]. Reinforced terraced fields method for fine tailings disposal was proposed in [23]. Statistical source identification method for groundwater downward the tailings dam was studied in [24], considering that identifying the possible sources of potential harmful metals in groundwater systems plays a crucial role in evaluating the potential risks to residents and local plant cover.

Recently, the safety monitoring of tailings dams has become a hot topic. Security monitoring items of tailings dams include displacement, saturation line, reservoir level, and dry beach [25]. Sjödahl et al. [26] proposed an internal erosion

process and anomalous seepage detection method for tailings dams based on resistivity measurements. Security monitoring systems for tailings dams based on global positioning system are discussed in [27, 28]. Several online monitoring strategies for tailings dams also have been researched and developed [25, 29–31]. Blight et al. [32] proposed a freshly deposited surfaces measurement method for two platinum tailings dams.

The length of dry beach is an important index affecting the safe operation of the tailings pond, because it not only affects the height of the tailings dam saturation line and the safety of the tailings dam but also decides the flood control ability of the dam. The shortage of the beach length will seriously affect the safety of the tailings ponds. With the injecting of the tail slurry, the dry beach length changes in real time. Researching and developing the real-time automatic measurement method for the dry beach length monitoring becomes an essential content of the tailings dam safety monitoring system.

Conventional instruments for dry beach length measurement are hard to obtain accurate results in real time. Two methods commonly used are described as follows. In the first approach, controlling the water level as low as possible before the rainy season to keep enough dry beach length, and setting red flags on the dry beach every 50 meters from the highest secondary dam based on the specific conditions of the dry beach. In the flood season, the dry beach length can be determined by cruise visual check. In the second approach, the dry beach slope is assumed to be uniform, and the length of dry beach can be calculated by the difference of reservoir water level elevation and the beach elevation. The disadvantage of the previous two approaches is obvious. The first method cannot achieve automatic measurement. As for the second method, the measurement error can be very large, because the dry beach slope is not evenly made. There also exist automatic noncontact measurement technology and equipment for dry beach length measurement, such as deploying multiple automatic altimeters in the center of ponds to measure the dry beach elevation automatically. An altimeter is consisted of grating measuring system, wireless data transmission modules, solar panels, battery, and so forth. But as a result of constant injection of slurry and changing of beach surface, altimeters need to be made regular layout again, otherwise they will be buried and cannot work normally.

In this paper, a novel online measurement method for dry beach length is proposed based on photogrammetric monitoring. The main work is divided into two parts. The first part refers to the measurement preparation work, and the second part refers to dry beach length calculation by the vision measurement technology. Preparation works mainly include camera calibration and place markers at the scene of the measurement. In the vision measurement process, firstly, an image taken by the camera is isolated as the dry beach area and the reservoir water surface area through image processing. Then the locations of the markers in the image are extracted, and finally, the dry beach length is calculated according to the parameters extracted.

2. Basic Principles of Photogrammetric Monitoring for Dry Beach Length

Pinhole imaging model is shown in Figure 1 [33]. The focal length of the camera is set to f, and the origin of coordinates is set as the optical center of the camera. The coordinates of the point in Q space are (X, Y, Z) and its corresponding points on the imaging plane are (x, y, f). According to the principle of pinhole imaging, the following equation can be obtained:

$$x = \frac{fX}{Z}, \qquad y = \frac{fY}{Z}. \tag{1}$$

Assume that two points in Q space are (X_1, Y_1, Z_1), (X_2, Y_2, Z_2), and their coordinates in the image plane are (x_1, y_1) and (x_2, y_2), respectively. In Q space, the distance between two points can be calculated as

$$D = \sqrt{(X_1 - X_2)^2 + (Y_1 - Y_2)^2 + (Z_1 - Z_2)^2}. \tag{2}$$

When $Z_1 \approx Z_2 = Z$, from (1) and (2), the following equations can be obtained:

$$D = \frac{Z\sqrt{(x_1 - x_2)^2 + (y_1 - y_2)^2}}{f}, \tag{3}$$

$$f = \frac{Z\sqrt{(x_1 - x_2)^2 + (y_1 - y_2)^2}}{D}, \tag{4}$$

$$Z = \frac{Df}{\sqrt{(x_1 - x_2)^2 + (y_1 - y_2)^2}}. \tag{5}$$

When the space distance between two points, distances from two points to the camera, and the image of the two points in the image plane are known, the camera focal length can be calculated from (4). According to (5), when the focal length of the camera, the actual size of the measured object, and the size in the image plane of the measured object are already known, the distance from the camera to the object can be calculated.

The method adopted is assisted by four marking rods in dry beach area. It should ensure that the four marking rods form a rectangle and keep the camera lens in the middle of the rectangle formed by the marking rods. Because the actual dry beach surface can be approximated as a plane, you can determine the water line by the points of four bars, and the dry beach is approximately thought to be in the same plane. Figure 2 shows the layout of the marker rods and the camera. The red points represent the marking rods, and the blue line is called water line, which represents the boundary of the dry beach and the water surface. LP1, LP2, RP1, RP2, dry beach, and the water line are in the same plane. By the points LP1 and LP2, we can define line LL, and the line LL intersects with the water line at point CL. By the points RP1 and RP2, we can define line RL, and the line RL intersects with the water line at the point CR. The distance between CL and CR is equal to the distance between RP1 and LP1.

According to the invariance of X-ray imaging, a point in space is still a point on the imaging plane, and a straight line

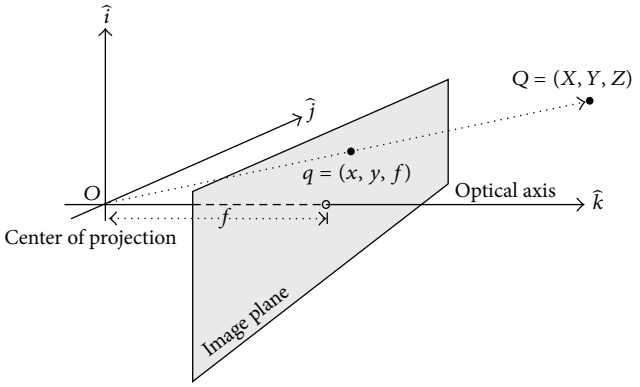

Figure 1: Pinhole imaging model.

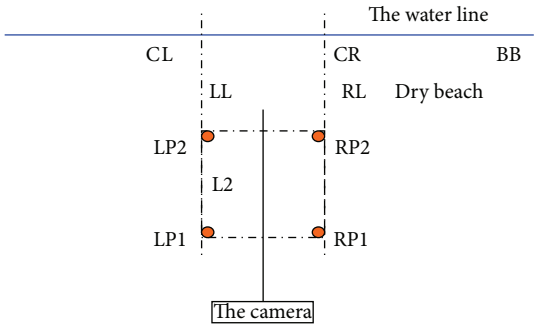

Figure 2: Measurement schemes.

in space is still a straight line on the imaging plane. Therefore, two points in the space corresponds to two image points, which determine a straight line on the imaging plane [34].

The principle can be described as follows.

Theorem 1. *Supposing that P1 and P2 are two points in the space and p1 and p2 are two points in the camera image plane, the image of the space straight line between P1, P2 is necessarily the straight line between p1 and p2 on the imaging plane.*

Figure 3 is a picture corresponding to the layout of Figure 2. In this figure, l1 and l2 are corresponding to LP1 and LP2 in Figure 2, and r1 and r2 are corresponding to RP1 and RP2 in Figure 2. According to Theorem 1, l1 and l2 determine the line corresponding to the line LL, and r1 and r2 determine the line corresponding to the line RL in the schematic diagram. Therefore, CL and CR correspond to the imaging points cl and cr, respectively. Because LL and RL are parallel to each other, the distance between CL and CR is equal to the distance between LP1 and RP1. This distance must be determined and measured when setting up marking rods. To calculate the distance between the camera and the boundary line, the critical problems are determination of the camera focal length and calculation of the pixel coordinates of cl and cr. Through (4), the camera focal length can be calculated, and through image processing technique, the pixel distance between cl and cr can be obtained. Then the distance between the camera and the boundary can be calculated from (5).

Figure 3: Layout of the mark poles.

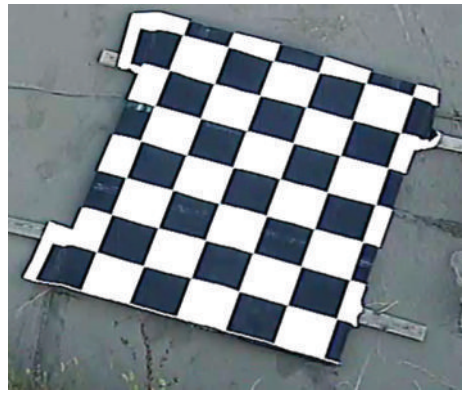

Figure 4: International chess calibration plate.

3. Measurement Steps

3.1. Camera Intrinsic Parameter Calibration. In image measurement process and machine vision applications, in order to determine the interrelation between the object surface geometry in three-dimensional space with the corresponding points in the image, it is necessary to establish the camera imaging geometric model, and the geometric model is determined by the camera parameters.

These parameters must be obtained through experiments and calculation, and the process of solving these parameters is called camera calibration. Both in image measurement and machine vision applications, camera parameter calibration work is a critical factor that influences the calibration results. Calibration precision and stability of the calibration algorithm directly affect the results accuracy of camera work. Therefore, completing the camera calibration is a premise to proceed to the next steps, and improving the calibration accuracy is the key of scientific research work.

The distortion of the camera in the process of imaging is usually unavoidable, and radial distortion is the main part of camera lens distortion. Taking optical axis as the center and its image coordinate as the reference point, radial distortion is proportional to the square of the distance from the point to the reference point. Only considering the second order of lens distortion, radial distortion can be described as

$$\begin{aligned} u - u_0 &= \left(u' - u_0\right)\left(1 + k_u r^2\right), \\ v - v_0 &= \left(v' - v_0\right)\left(1 + k_v r^2\right), \end{aligned} \tag{6}$$

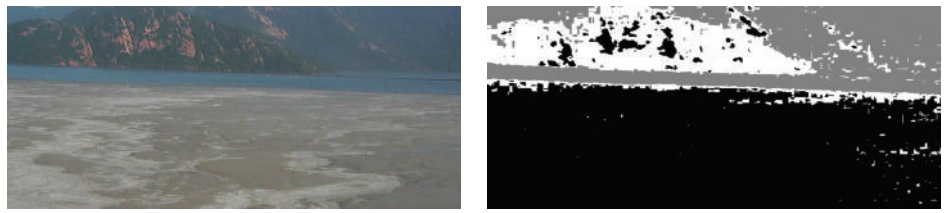

(a) (b)

Figure 5: Example of image segmentation by k-means clustering algorithm: (a) original image; (b) image after segmentation.

where (u', v') is the ideal arthroscopic image coordinate without distortion, (u, v) is the actual image coordinate, (u_0, v_0) is the image coordinates of the optical axis center, r is the distance between the image point to the reference point, and k_u, k_v are the second-order distortion coefficients along the directions u and v. Camera distortion parameters can be obtained by calibration to the camera intrinsic parameters.

This paper adopts the camera calibration method proposed by Zhang [35]. The plane calibration method proposed by Zhang is a kind of method between the traditional calibration methods and self-calibration methods. It avoids some disadvantages of the traditional methods, such as the high requirement for equipment and complicated operation. Meanwhile, like the self-calibration method, it has the advantage of high accuracy. The steps for camera calibration procedure are described as follows. (1) Make a pane of a chess board template with the size 20 cm × 20 cm for each cell and stick it on a flat surface, as shown in Figure 4. (2) Take several template images from different angles. (3) Detect the feature points in the international chess calibration plate. (4) Calculate the inner and outer parameters of the camera. (5) Calculate the distortion coefficient. (6) Optimization and refinement. The camera distortion parameters are obtained after camera calibration, and the distortion parameters can be used to correct the images taken by the camera.

3.2. Dry Beach and the Water Surface Areas Extraction. Due to the characteristics of dry beach area images differ from the characteristics of the water surface area images. Therefore, we can take advantages of regional segmentation method to extract the dry beach area and water surface area in the digital image. The edge of the water surface area is the boundary of the dry beach and the water. The intention of digital image segmentation is to segment the areas with different particular meanings. These areas are mutually disjoint, and each area meets the consistency of a particular area. Areas segmented by an excellent segmentation algorithm should satisfy the following conditions. (1) The partition of the image area should satisfy the requirement for uniformity and connectivity. The uniformity refers to the pixels, which should satisfy all the pixels in the same kind of similarity criterion based on the texture, color, and other characteristics. Connectivity refers to there exist paths for connecting any two points in the area. (2) There are notable differences between adjacent segmented regions. (3) The boundary of segmentation regions should be neat, and at the same time positioning accuracy of the edges should be ensured.

The image segmentation method based on k-means clustering algorithm is adopted. Because the clustering algorithm is concise and efficient, it is widely used in all kinds of clustering problems. Given a set of data points and the number of clusters k, k-means algorithm can classify the data points into k clusters based on a certain distance function. The parameter k is specified by the user. The steps of k-means clustering algorithm for image segmentation are described as follows.

(1) Transform the camera image from RGB color space to $L \times A \times B$ space. The $L \times A \times B$ space of the image can describe the regional characteristics better than RGB color space, and the values of A and B in the $L \times A \times B$ space are regarded as the characteristic values for each point in the image.

(2) Set the number of clusters to be $k = 3$, and initialize the cluster centers. When camera is adopted to monitor the length of dry beach, the camera image area is mainly composed of dry beach, water, and other areas. Therefore, the number of clusters is set to be $k = 3$ when using the k-means clustering algorithm for image segmentation.

(3) Calculate the distance between each pixel and the clustering center. Each pixel is classified in accordance with the principle of minimum distance to the nearest clustering center. The clustering centers are calculated as mean values of cluster samples in each cluster.

(4) Repeat step (3) until the clustering centers no longer change.

Figure 5 is an example of image segmentation by k-means clustering algorithm. In Figure 5(a), the original image of tailings areas is taken by a camera. The k-means clustering algorithm for image segmentation is adopted to extract different regions. In Figure 5(b), the black part represents the dry beach area, the gray part represents the water surface area, and the white part represents the other area. It can be seen that the water surface area can distinguish different parts clearly. So the pixels of the water surface area can be adopted to extract the boundary.

3.3. Marking Rods Extraction. Marking rods are adopted in the visual measurement to determine two parallel lines. Then the distance from the camera to the dry beach can be measured by using the principle of that the distances between two parallel lines are equal. The positions of the marking rods should be extracted from the image accurately. We use

Table 1: Image templates of four marking rods.

Marking rods	1	2	3	4
Sign	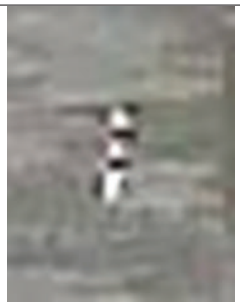	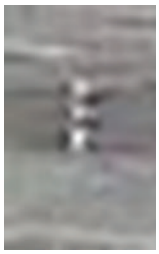	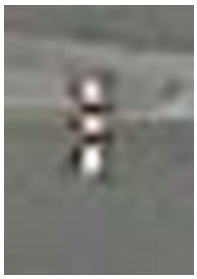	

the method of digital image template matching to locate the position of marking rods in the image. The image template is a small image already known. Template matching is a method used to search the goals in a big image. We can find the target and determine its location via calculating under the condition that the target has the same size, direction, and image with the template.

The principle of image template matching is described as follows. Firstly, the image template T ($m \times n$ pixels) is translated into the search graph S ($W \times H$ pixels), and the area that is covered by the image template is called subgraph S_{ij}. The indexes i and j are the coordinates in the search graph S. The search scope is $1 \le i \le W - m$ and $1 \le j \le H - n$. By comparing the similarity between T and S_{ij}, we can complete the template matching process. Similarity between image template T and subgraph S_{ij} can be measured as

$$D(i,j) = \sum_{p=1}^{m} \sum_{q=1}^{n} \left| S_{ij}(p,q) - T(p,q) \right|. \quad (7)$$

The procedure for images template matching has the following steps. (1) Extract the required image templates. Table 1 shows the image templates of four marking rods. (2) Calculate the similarity $D(i, j)$ between images and the template by (7). (3) Find the minimum similarity $D(i, j)$, and (i, j) is the position of the marker rod that we want to find.

The installation diagram of high-definition camera is shown in Figures 6 and 7. Figure 8 shows the positions of marking rods detected by template matching method.

3.4. Dry Beach Length Calculation. The water surface area and coordinates of marking rods can be obtained by regional segmentation of the image and identification of marking rods. As shown in Figure 9, the white color represents the water surface area, the red dots represent the marking rods, and the green lines are two parallel lines determined by marking rods. The intersection points of the two parallel lines with the water surface area are cl and cr, as shown in Figure 3. After calculating the distance between the two pixels, by using (5), we can calculate the dry beach length, which equals the distance from the boundary to the camera.

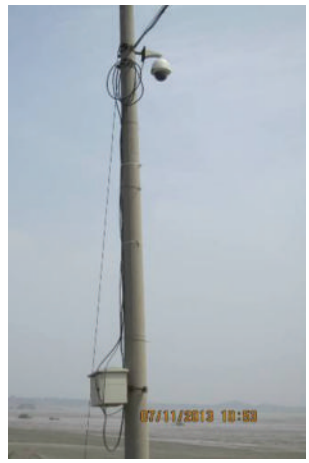

Figure 6: Installation diagram.

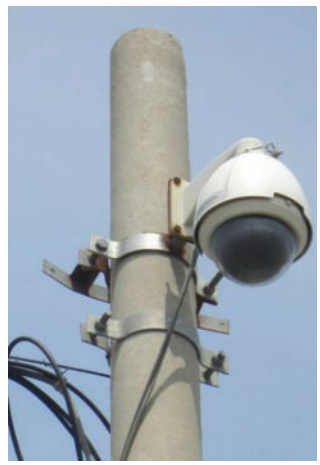

Figure 7: High-definition camera.

4. Experimental Results

Three experiments are performed to verify the proposed method for dry beach length measurement. In the three experiments, the distance between the camera and water line is set at 150 m, 200 m, and 300 m. This is achieved by moving the camera and marking rods. The measurement results of the experiments are shown in Table 2. It can be seen that when the distance is small, the error is also small, and

Table 2: The measurement results.

The actual distance (m)	The measured distance (m)	Relative error
150	147.8	1.46%
200	194.6	2.7%
300	309.7	3.2%

Figure 8: Extraction of marking rods.

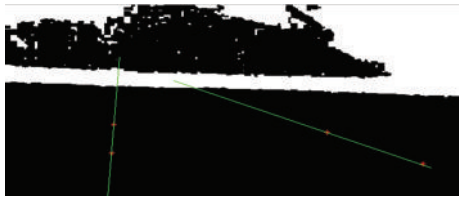

Figure 9: Water surface area and parallel lines determined by marking rods.

the error will increase with the rising of distance. When the actual distance is 300 m, the relative error is only 3.2%. Therefore, it still satisfies the requirement of measurement accuracy.

5. Conclusion

The dry beach length of a tailings dam is hard to be accurately measured automatically. In this paper, we propose a method for measuring real-time length of dry beach length by using an ordinary camera assisted with marking rods. When using the method, we should pay special attention to two items. (1) In order to meet the requirement of the measurement model, the four marking rods should be placed as a rectangle. Meanwhile, the optical axis of the camera should be placed at the axis of the rectangular. Then the assumption $Z_1 = Z_2$ in (1) can be satisfied. (2) In the paper, only two marking rods are used to determine a straight line, but in order to improve the measuring reliability and robustness, more marking rods can be used to determine the straight line. After extracting the positions of marking rods from the image, a curve fitting method can be applied to determine the straight line. Experimental results show that the proposed method has the advantages of convenient, accurate, and reliable performance, and the cost of measurement equipments is low.

Acknowledgments

This research was supported by National Natural Science Foundation of China under Grant nos. 51274053, 51109028, the State "Twelve Five" Science and Technology Support Projects under Grant no. 2013BAB02B00, the Natural Science Foundation of Liaoning Province under Grant no. L2011040, the State Scholarship Fund of China to pursue study in USA as a visiting scholar under Grant no. 201208210208, and Scientific Research Foundation of University of Science and Technology Liaoning

References

[1] P. C. Chang, A. Flatau, and S. C. Liu, "Review paper: health monitoring of civil infrastructure," *Structural Health Monitoring*, vol. 2, no. 3, pp. 257–267, 2003.

[2] Y. Q. Ni, X. W. Ye, and J. M. Ko, "Monitoring-based fatigue reliability assessment of steel bridges: analytical model and application," *Journal of Structural Engineering*, vol. 136, no. 12, pp. 1563–1573, 2010.

[3] Y. Q. Ni, X. W. Ye, and J. M. Ko, "Modeling of stress spectrum using long-term monitoring data and finite mixture distributions," *Journal of Engineering Mechanics*, vol. 138, no. 2, pp. 175–183, 2011.

[4] T. H. Yi, H. N. Li, and M. Gu, "Recent research and applications of GPS-based monitoring technology for high-rise structures," *Structural Control and Health Monitoring*, vol. 20, no. 5, pp. 649–670, 2013.

[5] T. H. Yi, H. N. Li, and M. Gu, "Wavelet based multi-step filtering method for bridge health monitoring using GPS and accelerometer," *Smart Structures And Systems*, vol. 11, no. 4, pp. 331–348, 2013.

[6] J. P. Lynch and K. J. Loh, "A summary review of wireless sensors and sensor networks for structural health monitoring," *Shock and Vibration Digest*, vol. 38, no. 2, pp. 91–130, 2006.

[7] S. N. Pakzad, G. L. Fenves, S. Kim, and D. E. Culler, "Design and implementation of scalable wireless sensor network for structural monitoring," *Journal of Infrastructure Systems*, vol. 14, no. 1, pp. 89–101, 2008.

[8] X. W. Ye, Y. Q. Ni, and J. H. Yin, "Safety Monitoring of railway tunnel construction using FBG sensing technology," *Advances in Structural Engineering*, vol. 16, no. 8, pp. 1401–1410, 2013.

[9] T. H. Yi, H. N. Li, and M. Gu, "Characterization and extraction of global positioning system multipath signals using an improved particle-filtering algorithm," *Measurement Science and Technology*, vol. 22, no. 7, Article ID 075101, 2011.

[10] T. H. Yi, H. N. Li, and X. Y. Zhao, "Noise smoothing for structural vibration test signals using an improved wavelet thresholding technique," *Sensors*, vol. 12, no. 8, pp. 11205–11220, 2012.

[11] F. Kang, J. J. Li, and S. Liu, "Combined data with particle swarm optimization for structural damage detection," *Mathematical Problems in Engineering*, vol. 2013, Article ID 416941, 10 pages, 2013.

[12] F. Kang, J. Li, and Q. Xu, "Damage detection based on improved particle swarm optimization using vibration data," *Applied Soft Computing Journal*, vol. 12, no. 8, pp. 2329–2335, 2012.

[13] F. Kang, J. Li, and Q. Xu, "Structural inverse analysis by hybrid simplex artificial bee colony algorithms," *Computers and Structures*, vol. 87, no. 13-14, pp. 861–870, 2009.

[14] X. Wang, F. Kang, J. J. Li, and X. Wang, "Inverse parametric analysis of seismic permanent deformation for earth-rockfill dams using artificial neural networks," *Mathematical Problems in Engineering*, vol. 2012, Article ID 383749, 19 pages, 2012.

[15] M. Rico, G. Benito, A. R. Salgueiro, A. Díez-Herrero, and H. G. Pereira, "Reported tailings dam failures. A review of the European incidents in the worldwide context," *Journal of Hazardous Materials*, vol. 152, no. 2, pp. 846–852, 2008.

[16] M. Rico, G. Benito, and A. Díez-Herrero, "Floods from tailings dam failures," *Journal of Hazardous Materials*, vol. 154, no. 1–3, pp. 79–87, 2008.

[17] R. S. Sharma and T. S. Al-Busaidi, "Groundwater pollution due to a tailings dam," *Engineering Geology*, vol. 60, no. 1–4, pp. 235–244, 2001.

[18] T. Wang, Y. Zhou, Q. Lv, Y. Zhu, and C. Jiang, "A safety assessment of the new Xiangyun phosphogypsum tailings pond," *Minerals Engineering*, vol. 24, no. 10, pp. 1084–1090, 2011.

[19] G. Yin, G. Li, Z. Wei, L. Wan, G. Shui, and X. Jing, "Stability analysis of a copper tailings dam via laboratory model tests: a Chinese case study," *Minerals Engineering*, vol. 24, no. 2, pp. 122–130, 2011.

[20] A. T. Özer and L. G. Bromwell, "Stability assessment of an earth dam on silt/clay tailings foundation: a case study," *Engineering Geology*, vol. 151, pp. 89–99, 2012.

[21] M. T. Zandarín, L. A. Oldecop, R. Rodríguez, and F. Zabala, "The role of capillary water in the stability of tailing dams," *Engineering Geology*, vol. 105, no. 1-2, pp. 108–118, 2009.

[22] X. Jianbin, F. Jing, L. Wenlian et al., "Dynamic stability of the tailings dam under high intensity seismic load coupled with the effect of seepage," *Disaster Advances*, vol. 5, no. 4, pp. 816–821, 2012.

[23] Z. Wei, G. Yin, G. Li, J. G. Wang, L. Wan, and L. Shen, "Reinforced terraced fields method for fine tailings disposal," *Minerals Engineering*, vol. 22, no. 12, pp. 1053–1059, 2009.

[24] M. Kargar, N. Khorasani, M. Karami, G. Rafiee, and R. Naseh, "Statistical source identification of major and trace elements in groundwater downward the tailings dam of Miduk Copper Complex, Kerman, Iran," *Environmental Monitoring and Assessment*, vol. 184, no. 10, pp. 6173–6185, 2012.

[25] G. Yu, C. Song, J. Zou et al., "Applications of online monitoring technology for tailings dam on digital mine," *Transactions of Nonferrous Metals Society of China*, vol. 21, supplement 3, pp. s604–s609, 2011.

[26] P. Sjödahl, T. Dahlin, and S. Johansson, "Using resistivity measurements for dam safety evaluation at Enemossen tailings dam in southern Sweden," *Environmental Geology*, vol. 49, no. 2, pp. 267–273, 2005.

[27] J. Hu and X. Liu, "Design and implementation of tailings dam security monitoring system," in *Proceedings of the 1st International Symposium on Mine Safety Science and Engineering (ISMSSE '11)*, vol. 26, pp. 1914–1921, October 2011.

[28] W. Li and C. Wang, "GPS in the tailings dam deformation monitoring," in *Proceedings of the 1st International Symposium on Mine Safety Science and Engineering (ISMSSE '11)*, vol. 26, pp. 1648–1657, October 2011.

[29] Q. Li, Y. Wang, and G. Li, "Tailings dam breach disaster online monitoring method and system realization," in *Proceedings of the 1st International Symposium on Mine Safety Science and Engineering (ISMSSE '11)*, vol. 26, pp. 1674–1681, October 2011.

[30] E. Sun, X. Zhang, and Z. Li, "The internet of things (IOT) and cloud computing (CC) based tailings dam monitoring and prealarm system in mines," *Safety Science*, vol. 50, no. 4, pp. 811–815, 2012.

[31] Z. H. Ouyan, "Research, development and application of surface displacement automatic monitoring system of tailings dam," *Advanced Materials Research*, vol. 422, pp. 304–309, 2012.

[32] G. Blight, A. Copeland, P. Jardine et al., "Measurements on freshly-deposited surfaces of two platinum tailings dams," *Journal of the Southern African Institute of Mining and Metallurgy*, vol. 112, no. 11, pp. 911–917, 2012.

[33] G. J. Zhang, *Visual Measurement*, Science press, Beijing, China, 2008.

[34] R. Hartley and A. Zisserman, *Multiple View Geometry in Computer Vision*, Cambridge University Press, Cambridge, UK, 2004.

[35] Z. Zhang, "Flexible camera calibration by viewing a plane from unknown orientations," in *Proceedings of the Seventh IEEE International Conference on Computer Vision (ICCV '99)*, vol. 1, pp. 666–673, September 1999.